Unwinding of a single quantized vortex from a wire

K. W. Schwarz
IBM Research Division, Thomas J. Watson Research Center, Yorktown Heights, New York 10598
(Received 13 July 1992)

The dynamical behavior of a quantized vortex partially attached to a wire is studied theoretically, with the aim of interpreting recent experiments on quantized circulation in superfluid ^{3}He-B. The geometry considered consists of a thin wire running parallel to the axis of a circular cylinder enclosing the wire. The circulation is assumed to run part way up the wire, and then to enter the fluid as a free vortex which eventually terminates on the outer wall. It is found that such a vortex achieves a state of steady precession around the wire, accompanied by a steady unwinding motion down the wire due to frictional effects. For an off-center wire, both the precession rate and the unwinding rate develop oscillatory components. Various particulars, such as the effects of friction, of moving the wire off center, and of pinning, are investigated. Excellent agreement is obtained between experiment, analytical theory, and numerical calculations.

I. INTRODUCTION

One of the basic assumptions of superfluid dynamics is that quantized vortex lines behave like idealized classical vortex filaments subject to a frictional force acting on the core. This semiclassical picture was first combined with the two-fluid model of Landau to describe vortex arrays in rotating superfluid ^{4}He,[1] and has ever since provided the basic phenomenology assumed to underlie the macroscopic flow properties of the superfluid. Although there does not appear to be any serious reason to question this assumption, it is very difficult to observe individual quantized vortices. Thus, the only direct, quantitative demonstration of the validity of the semiclassical approximation has come from measurements made on the propagation of quantized vortex rings.[2] A recent remarkable experiment[3] on the behavior of a single quantum of circulation trapped on a wire now provides a stringent test of this whole approach.

Using a method pioneered by Vinen,[4] and later also utilized by Karn, Starks, and Zimmermann,[5] the circulation properties of superfluid ^{4}He are studied by setting the fluid into rotation about a fine stretched wire. A finite circulation of the fluid about the wire causes a lift force to be exerted on the wire when it is set into vibration, leading the plane of vibration of the wire to precess. As was pointed out by Vinen, it is possible for the circulation to be only partially trapped on the wire, peeling off into the fluid as a free vortex at some point along its length. The precession rate of the wire, and hence the apparent circulation, will be appropriately reduced when this occurs. In measurements on superfluid ^{4}He, it was found that the circulation is indeed quantized in the expected units of h/m_4, but signals indicating a partially attached quantized vortex were often observed. Such flow states tended to persist indefinitely, indicating that the free vortex was permanently hung up on some local protrusion on the wire or on the walls of the rotating container.

The vibrating-wire technique has now been extended to investigate the circulation properties of ^{3}He-B. The dynamical features associated with quantized vortices are expected to be much the same as for superfluid ^{4}He, except that the quantum of circulation $\kappa_3 = h/2m_3 \simeq 0.665 \times 10^{-3}$ is somewhat smaller, and the vortex core size of about 1000 Å is 3 orders of magnitude larger than that found in ^{4}He. Davis *et al.*[6] have used this technique to measure the quantum of circulation in ^{3}He-B. More recently, Zieve *et al.*[3] have found that the measured circulation tends to decay away, typically over a period of many hours. They observe this process to be accompanied by a striking periodic modulation of the precession rate of the wire, i.e., of the effective amount of circulation remaining on the wire. Figure 1 reproduces the relevant data from their paper.

The authors of Ref. 3 interpret their observations as reflecting the dynamical properties of a partially attached quantized vortex, configured as shown schematically in Fig. 2. On the surmise that such a vortex undergoes a

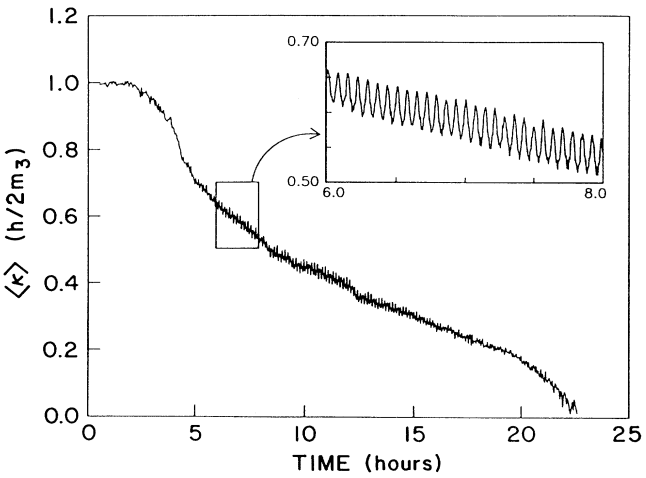

FIG. 1. Measured effective circulation as a function of time [after Zieve *et al.* (Ref. 3)].

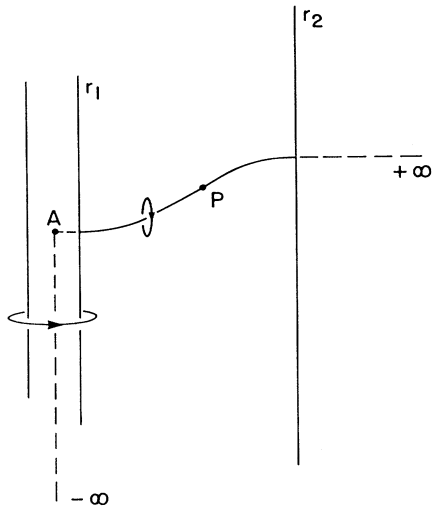

FIG. 2. Schematic geometry of the partially attached vortex. The circulation travels partway up the inner wire (radius r_1) and then enters the fluid as a free vortex, terminating on the containing cylinder (radius r_2). There is no circulation about the wire above A. The dashed lines indicate how the vortex is continued into the boundary in order to evaluate the Biot-Savart integral.

rigid precession about the central wire, they find excellent agreement with experiment. It is the purpose of our paper to show that it is indeed possible to explain the observed behavior in terms of the quasiclassical dynamics of a partially attached vortex, and to extend the simple picture of a precessing vortex in several ways.

II. BASIC CALCULATION

In the absence of normal fluid friction, the dynamics of a quantized vortex is determined by the Kelvin circulation theorem, which states that the vortex core must be convected along with whatever translational velocity field it sees. This velocity field, in turn, arises from the presence of the vortex itself, so that the motion of the vortex filament at any instant is determined solely by its own configuration. The task of finding the motion of the vortex shown in Fig. 2 thus boils down to finding the velocity field that it generates at its own core. This problem is very similar in spirit to the problem of a vortex terminating on a hemispherical bump, the complete solution of which has been presented elsewhere.[7] The reader is referred to Ref. 7 for a more detailed discussion of some of the following points.

The velocity field generated by a vortex filament in an infinite medium can be calculated using the Biot-Savart law *provided* the filament is continuous. To apply the Biot-Savart law to the configuration shown in Fig. 2 therefore requires one to continue the filament into the boundary in some fashion, the integration being carried out over the entire filament so defined. The field $\mathbf{v}_\omega$ calculated in this way does not account for the presence of the wire or the outer container. An irrotational field $\mathbf{v}_b$ satisfying the condition $\hat{n}\cdot(\mathbf{v}_b-\mathbf{v}_\omega)=0$ on these surfaces must therefore be added to satisfy the requirement that there be no fluid flow into any solid surface. The sum $\mathbf{v}_\omega+\mathbf{v}_b$ then generates the motion of the vortex.

The onerous part of doing a calculation like this is to find $\mathbf{v}_b$. In the present situation, however, $\mathbf{v}_b$ at the core can be made small by an intelligent choice of how the vortex is continued into the boundaries. In Fig. 2, the portion from $-\infty$ to A generates a contribution to $\mathbf{v}_\omega$ which has no normal component into the boundaries and hence generates no boundary correction.[8] The boundary field generated by the part running from A to $+\infty$ is large in some regions, but happens to be small where the vortex core is located. It is, in fact, easily seen from symmetry that, if the vortex runs out as a radial straight line, the value of $\mathbf{v}_b$ at the core is identically zero. Since the steady-state configuration achieved by the partially attached vortex will turn out to deviate only slightly from this, $\mathbf{v}_b$ can be entirely neglected to a satisfactory order of accuracy.

Given that $\mathbf{v}_b$ is neglected, the velocity acting on the vortex core at a given point P is obtained simply by integrating the Biot-Savart law over the vortex shown in Fig. 2. Because of the well-known logarithmic divergence in the velocity that a curved vortex-filament generates on itself, the integration must be broken up into a locally self-induced motion, arising from the part of the vortex near P, and a nonlocal correction term arising from the Biot-Savart integral over those parts of the vortex that are farther away:[7]

$$\dot{\mathbf{s}}_0=\frac{\kappa}{4\pi}\mathbf{s}'\times\mathbf{s}''\ln\left[\frac{2(l_+l_-)^{1/2}}{e^{1/4}a_0}\right]+\frac{\kappa}{4\pi}\int'\frac{(\mathbf{s}_1-\mathbf{s})\times d\mathbf{s}_1}{|\mathbf{s}_1-\mathbf{s}|^3}\ . \tag{1}$$

Here $\mathbf{s}(\xi)$ describes the vortex configuration, κ is the quantum of circulation, a_0 is the vortex core radius, the primes denote the derivative with respect to the arc length, and l_+ and l_- are the lengths of the elements used in evaluating the local configuration. The prime on the integral indicates that it is taken so as to exclude l_+ and l_-. In the present geometry, the only important nonlocal contribution to the velocity acting at point P is the circulating field contributed by that part of the vortex ($-\infty$ to A) which is still on the wire, a contribution which can readily be evaluated analytically:

$$\mathbf{v}_\varphi(\delta)=\frac{\kappa}{4\pi\delta}\left[\frac{1+\cos\zeta}{\sin\zeta}\right]\hat{\varphi}\ , \tag{2}$$

where ζ is the angle between the line from $-\infty$ to A and the line from A to P, δ is the distance from A to P, and $\hat{\varphi}$ is the unit vector into the figure in accord with the right-hand rule. Since ζ never differs much from $\pi/2$, one can further approximate $\mathbf{v}_\varphi$ by $(\kappa/4\pi r)\hat{\varphi}$, this being just half the field of a vortex running from $-\infty$ to $+\infty$. The other nonlocal terms are small and can be neglected. The accuracy of this approximation is optimized by setting the logarithm in Eq. (1) to $\ln(cr_2/a_0)$, where c is of order 1. Instead of an apparently very complicated problem in vortex dynamics, we now have the simple approximate

equation

$$\dot{\mathbf{s}}_0=\beta\mathbf{s}'\times\mathbf{s}''+(\kappa/4\pi r)\hat{\varphi}\ , \tag{3}$$

where $\beta=(\kappa/4\pi)\ln(cr_2/a_0)$. The errors made in approximating the velocity of the vortex sketched in Fig. 2 by this equation should be on the order of a few percent at most.

Equation (3) is not quite the whole story because a quantized vortex filament will also experience a frictional force per unit length due to the scattering of elementary excitations by the core. This force is approximated by

$$\mathbf{f}_\alpha=\kappa\rho_s\alpha(\mathbf{v}_n-\dot{\mathbf{s}}_0)_\perp\ , \tag{4}$$

where $\mathbf{v}_n$ is the drift velocity of the excitation gas and α is a temperature-dependent friction constant measuring the strength of the interaction. The ideal-fluid motion $\dot{\mathbf{s}}_0$ of the vortex is then modified to

$$\dot{\mathbf{s}}=\dot{\mathbf{s}}_0+\alpha\mathbf{s}'\times(\mathbf{v}_n-\dot{\mathbf{s}}_0)\ . \tag{5}$$

The frictional term is required in order for the superfluid to lose energy, and thus plays an important role both in allowing the partially attached vortex to reach a steady state of motion and in causing it to unwind from the wire. It is of some interest to include the possibility of uniform axial super and normal fluid velocities $\mathbf{V}_s$ and $\mathbf{V}_n$, and of normal fluid solid body rotation with an angular frequency Ω_n. The velocity of the vortex is then

$$\dot{\mathbf{s}}=\beta\mathbf{s}'\times\mathbf{s}''+\frac{\kappa}{4\pi r}\hat{\varphi}+V_s\hat{z}+\alpha\mathbf{s}'\times\left[V_n\hat{z}-V_s\hat{z}+\Omega_n r\hat{\varphi}-\beta\mathbf{s}'\times\mathbf{s}''-\frac{\kappa}{4\pi r}\hat{\varphi}\right]\ . \tag{6}$$

Figure 3(a) shows the result of a typical numerical calculation based on Eq. (6), with V_n, V_s, and Ω_n set equal to zero.[9] The calculation is started from an initial condition in which the vortex runs straight across from the wire to the outer wall. After some transient oscillations [Fig. 4(a)], the vortex reaches a new configuration which rotates as a rigid object and with a constant angular velocity Ω about the inner wire. These figures show that, at least for an on-center wire and small α, the vortex does not deviate greatly from a horizontal straight line, so that the approximations leading to Eq. (3) are justified. Because $\mathbf{v}_\varphi$ is weak, and the vortex is distorted only slightly, it is necessary to do the calculations in extended precision to obtain reliable results.

The velocity $\mathbf{v}_\varphi$ which drives the vortex around does not resemble solid body rotation, and it is worthwhile to consider how the uniform-rotation behavior attained in Fig. 4(a) comes about. As the radial line is first deformed by $\mathbf{v}_\varphi$, those parts of the vortex nearest to r_1 are swept around more rapidly than those far away. This generates a distortion of the straight vortex leading to a self-induced velocity $\beta\mathbf{s}'\times\mathbf{s}''$. Such distortions are efficiently propagated along the line in the form of helical waves[10] modifying the overall configuration. With no friction, the vortex will oscillate about some mean motion. With damping, however, it eventually settles down to a steady-state motion which cannot take any other form than a rigid, constant rotation of the vortex filament. In this limit, the vortex configuration has adjusted itself so that near the wire $\beta\mathbf{s}'\times\mathbf{s}''$ cancels out part of the circulating field $\mathbf{v}_\varphi$, while near the outer cylinder the two fields reinforce each other. It follows that the vortex must curve upward near the wire and downward near the outer wall.

For vanishing α, the steady-state vortex lies entirely in the r-z plane. For finite α, the situation is modified slightly since clearly the action of the frictional term in Eq. (5) would lead to a nonuniform downward motion when applied to a uniformly rotating vortex. The distortions caused by this nonuniformity lead to some further readjustment of the vortex configuration, which now develops a small excursion out of the r-z plane. The result is an additional self-induced term which corrects the friction-induced term to yield a uniform downward motion of the vortex.

To conclude this section, we comment briefly on dynamical scaling[11] as it relates to Eq. (6). With the usual substitutions $t_0=\beta t$, $v_0=v/\beta$, one obtains a reduced equation wherein the nonlocal term appears in the form $(\kappa/\beta)/(4\pi r)\hat{\varphi}$. If κ/β were constant, this reduced equation would have the property that any solution can be

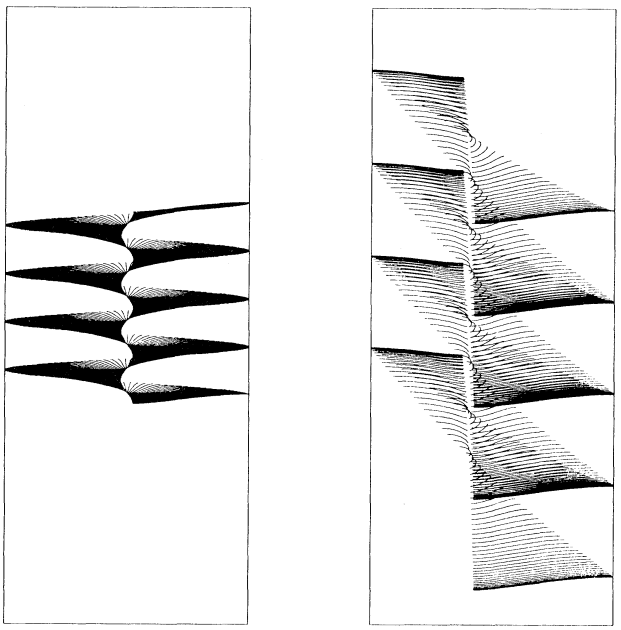

FIG. 3. Calculated steady-state motion, see from the side, of a partially attached vortex. The circulation points as shown in Fig. 2, and the precession is counter-clockwise when viewed from the top. (a) corresponds to $r_1=0.0005$ cm, $r_2=0.100$ cm, $\Delta=0.000$ cm, and $\alpha=0.10$. (b) differs only in that $\Delta=0.020$ cm. (Δ is the displacement of the wire axis from the center.) Here the motion starts at the topmost point on the *right*. Note that for (b) the vortex first swoops upwards as it precesses around to the short side. All vortex sequences shown in this paper are stepped by constant time intervals.

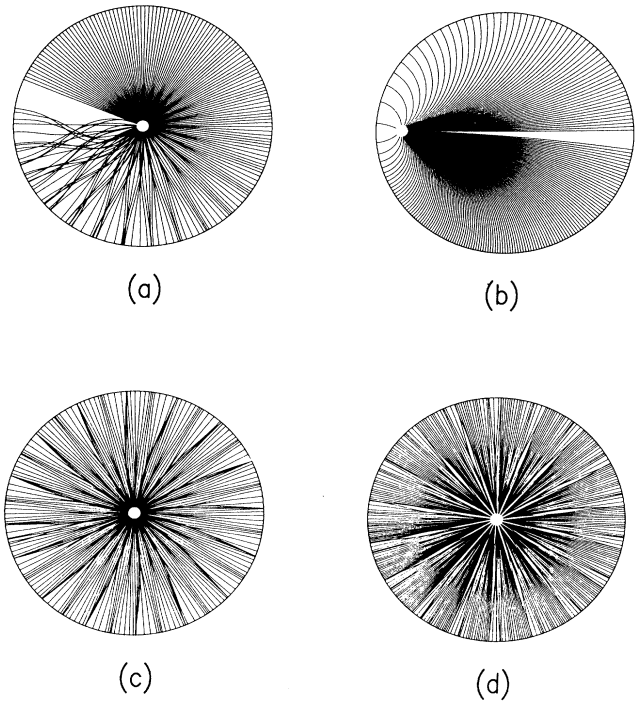

FIG. 4. Top view of vortex precessing under various circumstances: (a) transient oscillations of a vortex coming into steady-state rotation (standard configuration, $\alpha=0.03$); (b) motion with a highly eccentric wire placement, corresponding to the middle curve of Fig. 10; (c) motion with pinning on the outer wall (critical angle 10°, path length 4×10^{-2} cm); (d) motion with pinning on the inner wire (critical angle 20°, path length 4×10^{-3} cm).

scaled by simultaneously multiplying all spatial dimensions by λ, all velocities by λ^{-1}, and all times by λ^2. Because β varies logarithmically with λ, there is, in fact, no such scaling. The variation is very slow, however, so that the above scaling property exists in an approximate sense. With a core radius of 1000 Å, changing scales by a factor of 10 results in a deviation of order 10% from perfect scaling.

III. ANALYTICAL APPROXIMATIONS

We describe the detached part of the vortex by the curve $\varphi=\varphi(r,t)$, $z=z(r,t)$, and associate the instantaneous velocity $\dot{\mathbf{s}}$ of Eq. (6) with each point on this curve. The equations governing the time evolution of the vortex are then

$$\frac{\partial\varphi}{\partial t}+\dot{s}_r\frac{\partial\varphi}{\partial r}=\frac{\dot{s}_\varphi}{r}\ , \tag{7a}$$

$$\frac{\partial z}{\partial t}+\dot{s}_r\frac{\partial z}{\partial r}=\dot{s}_z\ , \tag{7b}$$

and the condition of uniform helical motion reduces to $\partial\varphi/\partial t=\Omega$, $\partial z/\partial t=\dot{Z}$, where Ω and $\dot{Z}$ are constants to be determined. The components of $\dot{\mathbf{s}}$ can be evaluated from Eq. (6) by writing $\mathbf{s}=(r\cos\varphi, r\sin\varphi, z)$ and going through the algebra, where it must be remembered that since the independent variable r is not the arc length, the more general forms $(\partial\mathbf{s}/\partial r)/|\partial\mathbf{s}/\partial r|$ and $(\partial^2\mathbf{s}/\partial r^2)/|\partial\mathbf{s}/\partial r|^2$ must be used for $\mathbf{s}'$ and $\mathbf{s}''$, respectively. The rather complicated result is

$$\begin{aligned}\dot{s}_r=&\beta\lambda^{-3}[r\varphi' z''-(r\varphi''+2\varphi')z']\\&+\alpha\lambda^{-1}[(V_n-V_s)r\varphi'-\Omega_n rz'\cos\varphi\\&\quad-\beta\lambda^{-3}r\varphi'^2+(\kappa/4\pi r)z']\ ,\end{aligned} \tag{8a}$$

$$\begin{aligned}\dot{s}_\varphi=&-\beta\lambda^{-3}(z''+r\varphi'^2z')+(\kappa/4\pi r)\\&+\alpha\lambda^{-1}[-(V_n-V_s)+\Omega_n rz'\sin\varphi z'\\&\quad+\beta\lambda^{-3}(2\varphi'+r\varphi'')]\ ,\end{aligned} \tag{8b}$$

$$\begin{aligned}\dot{s}_z=&\beta\lambda^{-3}(2\varphi'+r\varphi''+r^2\varphi'^3)+V_s\\&+\alpha\lambda^{-1}[\Omega_n r(\cos\varphi-r\varphi'\sin\varphi)\\&\quad+\beta\lambda^{-3}z''-(\kappa/4\pi r)]\ ,\end{aligned} \tag{8c}$$

where $\lambda=(1+r^2\varphi'^2+z'^2)^{1/2}$, and the primes now denote the derivative with respect to r.

Retention of only terms to first order in $\partial\varphi/\partial r$ and $\partial z/\partial r$, i.e., in the deviation of the vortex from a straight radial line, in Eqs. (7a) and (7b) results in two linear equations which can easily be integrated to yield

$$\beta z'=\frac{\kappa}{4\pi}\ln r-\gamma(\Omega+\alpha^2\Omega_n)\frac{r^2}{2}+\alpha\gamma(\dot{Z}-V_n)r+c_z\ , \tag{9a}$$

$$\beta r^2\varphi'=\gamma\alpha(\Omega-\Omega_n)\frac{r^3}{3}+(\gamma\dot{Z}-V_s+\gamma\alpha^2V_n)\frac{r^2}{2}+c_\varphi\ , \tag{9b}$$

where $\gamma=(1+\alpha^2)^{-1}$. With the boundary conditions $\mathbf{s}'\cdot\hat{\varphi}=\mathbf{s}'\cdot\hat{z}=0$ at $r=r_1,r_2$ one then obtains the again rather complicated results

$$\Omega=\frac{[\kappa(1+\alpha^2)/2\pi]\ln(r_2/r_1)-\alpha^2\Omega_n[(r_2^2-r_1^2)-\frac{4}{3}(r_2^3-r_1^3)/(r_2+r_1)]-2\alpha(1+\alpha^2)(V_n-V_s)(r_2-r_1)}{[(r_2^2-r_1^2)+(4\alpha^2/3)(r_2^3-r_1^3)/(r_2+r_1)]} \tag{10}$$

$$\dot{Z}=-\frac{2\alpha}{3}(\Omega-\Omega_n)(r_2^3-r_1^3)/(r_2^2-r_1^2)+V_s-\alpha^2(V_n-V_s)\ . \tag{11}$$

A comparison of these predictions with representative numerical calculations is given in Figs. 5 and 6, which show differences of a few tenths of 1%. This is consistent with the residual numerical errors of our calculations. Equations (9a) and (9b) are trivially integrated to yield the vortex configuration. Figures 7 and 8 show the resulting dependence of the filament shape on the friction constant. Again, the numerically calculated configurations are in essentially perfect agreement. The consistency of analytical and computational results not

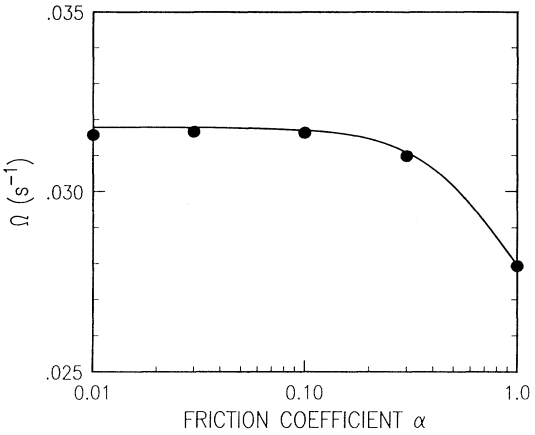

FIG. 5. Comparison of the analytical approximation for Ω [Eq. (10)] with representative numerical calculations, shown as dots. Here $r_1=0.005$ cm and $r_2=0.100$ cm.

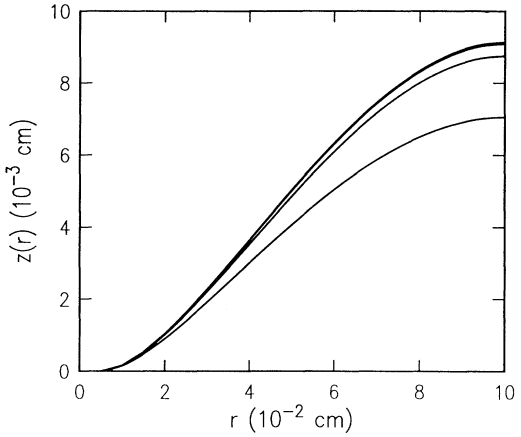

FIG. 7. Dependence of vertical variation on friction constant [from integrating Eq. (9a) analytically]. Starting from the bottom, the lines correspond to an α of 1.0, 0.3, 0.1, 0.03, and 0.01. The final three cannot be distinguished.

only provides a check on the accuracy of the computations, but also demonstrates the adequacy of the linearization approximation made in deriving Eqs. (10) and (11).

The approximate replacement of Eq. (2) by $(\kappa/4\pi r)\hat{\varphi}$ was introduced to facilitate the analytical treatment outlined above. As far as numerical calculations go, however, it is just as easy to use the more accurate form (2). We have performed such calculations for the standard on-center geometry[9] and find that the more accurate form (2) lowers Ω by about 4% at all values of the friction constant α. Thus, the error introduced by this particular approximation is small but not entirely negligible.

The experiment of Zieve *et al.*[3] corresponds to $\alpha\rightarrow 0$, $V_s=V_n=\Omega_n=0$. Then

$$\Omega=\frac{\kappa\ln(r_2/r_1)}{2\pi(r_2^2-r_1^2)}\ , \tag{12}$$

$$\dot{Z}=-\frac{2\alpha}{3}\Omega(r_2^3-r_1^3)/(r_2^2-r_1^2)\ . \tag{13}$$

These equations have already been proposed by Zieve *et al.* on the basis of a force-balance argument. Since α is quite small in the experiments, Eqs. (10) and (11) show that friction effects can be neglected. In addition, we learn that the leading-order effect of V_s is to wash the vortex along the $\hat{z}$ direction. The main effect of V_n-V_s is to change the precession frequency by an amount $-2\alpha(V_n-V_s)/(r_1+r_2)$. Most interestingly, a rotation of the normal fluid has the effect of changing the unwinding rate in the same way as the precession frequency. Thus, by setting the experiment into rotation again after the vortex has started to unwind, it should be possible to run the vortex up and down the wire in a controlled manner.

IV. FORCE-BALANCE ARGUMENTS

The authors of Ref. 3 give a clever argument for Ω which balances off the "net Magnus force" experienced by the free part of the vortex as it precesses against an "effective force" arising from the energy per unit length

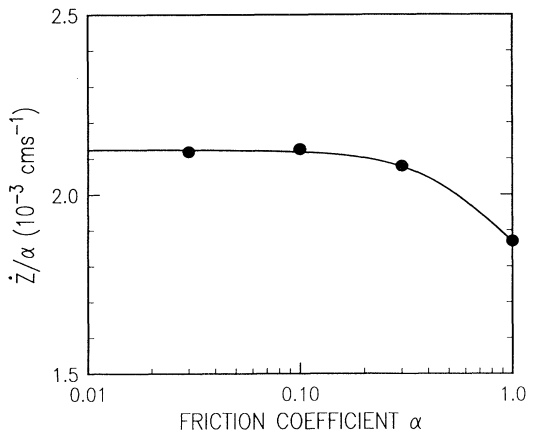

FIG. 6. Comparison of the analytical approximation for the unwinding rate [Eq. (11)] with numerical calculations.

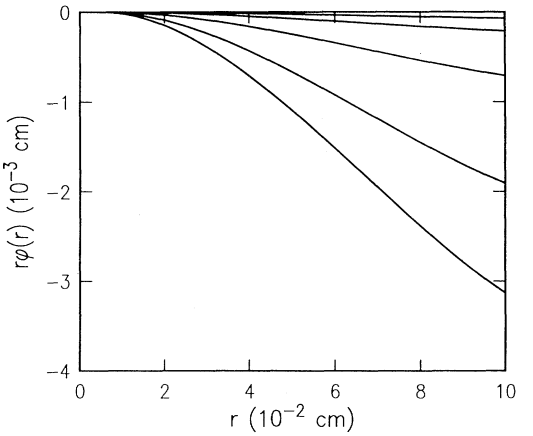

FIG. 8. Dependence of azimuthal variation on friction constant [from Eq. (9b)]. The displacement grows with α, and becomes quite large as $\alpha\rightarrow 1$. Starting from the bottom, the lines correspond to an α of 1.0, 0.3, 0.1, 0.03, and 0.01.

of the vortex trapped on the wire. Their discussion is presented in a language peculiar to the low-temperature literature, and it is at least of cross-cultural interest to translate it into more conventional fluid dynamical terms.

For simplicity, we assume that the normal fluid velocity is negligible. The quantity describing the flow of forces is then the momentum flux tensor

$$\pi_{ik}=p\delta_{ik}+\rho_s v_{si}v_{sk} \ . \tag{14}$$

The instantaneous velocities are determined by solving the vortex motion problem as outlined previously. The pressure p needed to complete the evaluation of π_{ik} can then be obtained from Bernoulli's equation:[12]

$$\frac{\partial\Phi}{\partial t}+\frac{p}{\rho_s}+\frac{1}{2}v_s^2=f(t) \ , \tag{15}$$

where Φ is the scalar potential $v_s=\nabla\Phi$. The velocity field in the neighborhood of the vortex core can always be written to leading order as the basic circulating field $(\kappa/2\pi a)\hat{\phi}$ plus a translational velocity $\mathbf{u}$ arising from various contributions such as the vortex curvature, the nonlocal vortex contributions, and boundary corrections. It is then easy to show from Eqs. (14) and (15) that if the vortex translates with a velocity $\dot{\mathbf{s}}$, the momentum flux into the vortex core per unit length of line is just

$$\mathbf{f}_l=\rho_s\boldsymbol{\kappa}\times(\dot{\mathbf{s}}-\mathbf{u}) \ , \tag{16}$$

i.e., simply the usual lift force. It is the content of the computational approach outlined in Sec. II that, since the vortex core has negligible inertia, it cannot absorb or supply any momentum. Hence, in the absence of external forces such as $\mathbf{f}_\alpha$ acting on the vortex core, $\mathbf{f}_l$ must be zero and the vortex must everywhere translate along with the local fluid velocity $\mathbf{u}$.

One can *artificially* separate Eq. (16) into a force that would be felt were the vortex translating through a fluid that is somehow adjusted to have no translational velocity $\mathbf{u}$ at the core (the $\dot{\mathbf{s}}$ contribution or the "net Magnus force" of Zieve *et al.*[3]), and the force that would be exerted by the fluid on the vortex were it held stationary (the $-\mathbf{u}$ contribution). For the uniformly precessing vortex it is easy to show that the total $\dot{\mathbf{s}}$ contribution in the vertical direction is $\rho_s\kappa\Omega(r_2^2-r_1^2)/2$, independently of the shape of the filament. The $\mathbf{u}$ contribution, on the other hand, can be evaluated by the following trick. If the vortex were to be held stationary, say by a wire passing along the core, the total vertical force that the fluid would exert on the bottom of the bucket (ignoring gravity) plus the force it would exert on the vortex would have to equal zero (the total momentum of the fluid is not changing, and the top of the bucket is assumed to be far enough away so that $\mathbf{v}$ is negligible there). According to Eq. (15), the force exerted on the bottom of the bucket in this time-independent situation is just

$$(\rho_s/2)\int v_s^2 dS=(\rho_s\kappa^2/4\pi)\ln(r_2/r_1) \ . \tag{17}$$

The negative of this, then, must be the force that would be felt by the mythical stationary vortex, independently of its configuration. When this is balanced against the $\dot{\mathbf{s}}$ term, Eq. (12) is recovered. The derivation shows that this is an exact result in the limit $\alpha\to 0$.

The argument just given can be adapted to the case of an off-center wire where, as we shall see in the next section, the vortex does not precess as a rigid object.[13] We note in Eq. (16) that $\rho_s\boldsymbol{\kappa}\times\dot{\mathbf{s}}dl\,\Delta t$ is just $\rho_s\kappa$ times the element of area swept out be a vortex element of length dl in term Δt. Since a vortex precessing around to its initial configuration sweeps out an area $\pi(r_2^2-r_1^2)$, no matter how it gets there, the time integral of the $\dot{\mathbf{s}}$ contribution to the total force acting on the vortex must be just $\rho_s\kappa\pi(r_2^2-r_1^2)$. The time integral of the $\mathbf{u}$ term is just $2\pi/\langle\Omega\rangle$ times the pressure integral over the bottom, except that now the velocity field appropriate to an off-center inner cylinder must be used in the integration. The field in this case is just the sum of $+\kappa$ and $-\kappa$ axial line vortices placed at positions

$$r_\pm=\frac{1}{2\Delta}(r_2^2-r_1^2+\Delta^2) \mp\frac{1}{2\Delta}\sqrt{(r_2^2-r_1^2+\Delta^2)^2-4\Delta^2 r_2^2} \ , \tag{18}$$

where Δ is the distance by which the wire axis is displaced from the center. Integration over the resulting flow pattern then gives

$$\langle\Omega\rangle=\frac{\kappa}{2\pi(r_2^2-r_1^2)}\cosh^{-1}\left[\frac{r_2^2+r_1^2-\Delta^2}{2r_1r_2}\right] \tag{19}$$

as the generalization of Eq. (12) for the $\alpha\to 0$ limit.

As regards the actual situation, it is important to understand that it is not time independent, and that in the limit $\alpha\to 0$ neither the processing vortex nor the bottom surface of the bucket feel *any* net force. The vortex is precessing precisely because it must maintain $\mathbf{f}_l$ equal to zero along its entire length. As it precesses, it generates a $\partial\Phi/\partial t$ term which exactly cancels out the $\rho_s v_s^2/2$ contribution to the pressure when it is integrated over the bottom of the bucket, or over any other surface spanning the bucket below the free vortex.

While Eq. (12) has been seen to follow from a force-balance argument, Eq. (13) can be derived from energy conservation by balancing the work done by the precessing vortex because of normal fluid friction against the energy per unit length of the trapped vortex. Unlike the expression for Ω, this *does* depend on the configuration of the vortex, even in the limit $\alpha\to 0$, so that Eq. (13) is only a first approximation.

V. OFF-CENTER WIRE

Because it is rotationally symmetric, the motion shown in Fig. 3(a) will not, in fact, produce an oscillating signal. The oscillations observed by Zieve *et al.*[3] arise from the fact that their wire was placed substantially off center. If it is assumed that the vortex remains more or less straight as it rotates around the off-center wire, then it will become longer and shorter as it moves around. Conservation of energy would then require the point of attachment to move up and down the wire, giving rise to an oscillating component in the measured effective circulation.

Computations done with an increasingly eccentric wire placement illustrate a number of interesting features. A typical calculation using a moderately off-center wire [Fig. 3(b)] shows that the vortex develops a significant oscillating curvature when viewed along the z axis. This gives rise to an additional vertical self-induced term $\beta \mathbf{s}' \times \mathbf{s}''$, and thus generates the vertical oscillations adduced in the previous paragraph and observed experimentally. The rate of precession also develops an oscillatory component, so that the observed oscillating signal becomes increasingly anharmonic as the wire is moved farther off center. Because the vortex travels farther when it is oscillating, the average unwinding rate $\langle \dot{Z} \rangle / \alpha$ will be affected to first order by the eccentricity. This effect will have to be taken into account when trying to extract the friction constant α from experimental data.

At high eccentricities, two additional features become very apparent. First, the velocity field of an off-center axial vortex must be supplemented by an image term as discussed previously. Both the **u**-term "force" acting on the bottom of the bucket and the energy per unit length of trapped circulation are greatly reduced. On the basis of momentum and energy balance, one would therefore expect the average rate of precession $\langle \Omega \rangle$ to decrease and the amplitude of the vertical oscillations to become very large. The latter, in turn, has a large effect on $\langle \dot{Z} \rangle / \alpha$. Figure 9 shows the calculated magnitude of these corrections in the limit $\alpha \to 0$. The top curve in Fig. 10 shows that the experimental "signal" for large eccentricities is expected to be strikingly anharmonic, an effect which should be accessible to observation.

The second feature is the increasing loss of symmetry of the precession curves at large eccentricities and finite α. This is due to the fact that when the vortex oscillates downward it feels a frictional force in the plus $\hat{z}$ direction. This, in turn, reduces the precession rate, the effect being the same as that which produces the $\alpha(V_n - V_s)$ term in Eq. (10). The opposite occurs when the vortex oscillates upwards. The effect is linear in α, and as seen in the middle curve of Fig. 10 and in Fig. 4(b), it becomes quite dramatic as α increases. In fact, the precession rate can easily decrease to *zero*, as shown by the bottom curve of Fig. 10. What is happening here is that the vortex reaches a limiting bowed shape, and propagates directly down the wire without precessing.

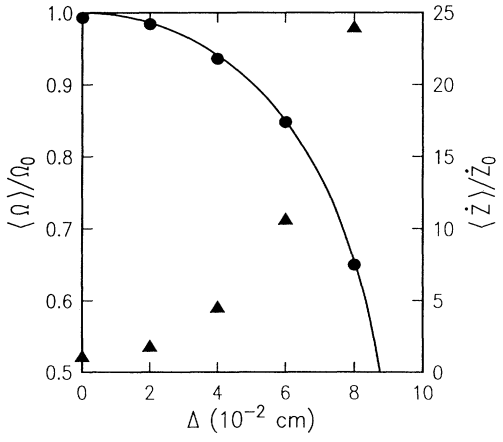

FIG. 9. Precession rate (dots) and unwinding rate (triangles) in the limit $\alpha \to 0$, calculated as a function of Δ, with $r_1 = 0.005$ cm and $r_2 = 0.100$ cm. The rates are normalized to the on-center values given by Eqs. (12) and (13). The solid line is the prediction of Eq. (19).

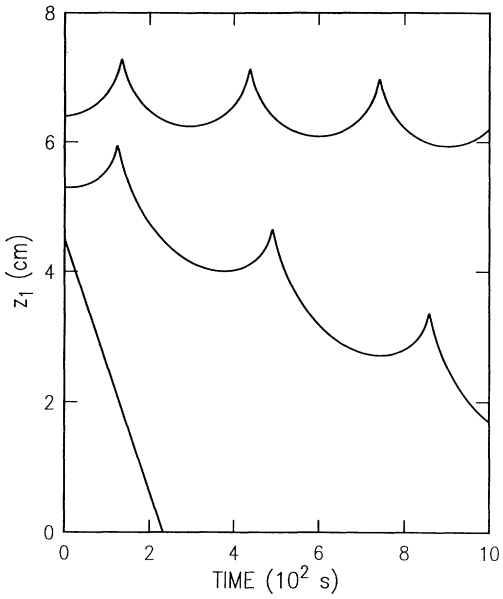

FIG. 10. Experimental signatures for a highly eccentric wire. Here $r_1 = 0.005$ cm, $r_2 = 0.100$ cm, and $\Delta = 0.080$ cm. The top cure is calculated with $\alpha = 0.03$, the middle with $\alpha = 0.06$, and the bottom curve with $\alpha = 0.10$.

VI. EFFECTS OF PINNING

A particular advantage of the numerical approach is that it permits exploration of complicated questions. Thus, we briefly discuss here the effects of surface roughness on the unwinding vortex. To represent the effects of roughness, we use the critical angle model,[7] in which the terminus of the vortex on the boundary is allowed to propagate for a certain distance, is then pinned, and is released again when the vortex (which comes in normal to the surface in the absence of pinning) has heeled over from the normal by a specified critical angle. The model is crude but descriptive, and the choice of the propagation path length and the critical angle allows a convenient parametrization of the nature of the surface. Thus, a surface containing only a few sharp asperities would correspond to a large free path length and a critical angle approaching $\pi/2$, while a small-scale waviness of the surface would be represented by a small free path length and a critical angle near zero.

Since a sharp asperity provides the strongest pinning and hence the clearest experimental signal, we have studied only the effects of large-angle roughness on the wire and on the outer boundary. As it turns out, for an on-center wire the critical angle cannot in any case be made very large: because the $\kappa/4\pi r \hat{\varphi}$ driving field is compara-

tively weak, pinning with even a moderate critical angle on either the inner or outer surface causes the vortex to hang up permanently. That is, once one end of the vortex is fixed, the vortex will spiral into a stationary configuration without ever suffering a sufficiently large deviation from normal incidence to become unpinned again. For our standard geometry of $r_1=0.005$ cm and $r_2=0.100$ cm, and with $\Delta=0$, the maximum critical angle for which interesting dynamical behavior occurs is about 12° for pinning on the outer surface and about 22° for the inner. Figures 4(c) and 4(d) show the kind of motion which occurs when there is pinning on the outer and inner surfaces, respectively. Although this looks reasonably dramatic, it is difficult to observe pinning events directly: the glitches introduced when the vortex hangs up and is released are of rather low amplitude. The effect of this kind of pinning on $\langle\Omega\rangle$ and $\langle\dot{Z}\rangle/\alpha$, however, appears to be both large and unpredictable. We find that the smooth-wall results $\Omega=0.0316$ s^{-1}, $\dot{Z}/\alpha=0.002\,13$ cm s^{-1} are modified to 0.0265 s^{-1}, 0.003 44 cm s^{-1} for the case shown in Fig. 4(c), and to 0.0179 s^{-1}, 0.001 81 cm s^{-1} for pinning on the inner wall [Fig. 4(d)]. The good agreement (discussed below) between the experimentally observed value of Ω and the smooth-wall theory indicates that surface roughness effects are, in fact, not important in the actual experiment, and we have not investigated these effects further, except as discussed in the next section.

VII. CALCULATIONS FOR THE EXPERIMENTAL CASE

The actual geometry quoted by Zieve *et al.*[3] is $r_1=(8\pm0.8)\times10^{-4}$ cm, $r_2=(1.480\pm0.006)\times10^{-1}$ cm, and $\Delta=(0.35\pm0.05)\times10^{-1}$ cm. If one estimates a friction constant from the inset of Fig. 1 and the results of Sec. V, one obtains a value of about 0.018. From Eq. (18), the theoretically predicted value of Ω is 0.0249 s^{-1}. The friction correction to this can be estimated from Eq. (10) to be of order 0.01% and is hence totally negligible.

Numerical calculations of the vortex motion become extremely time consuming when the inner radius and the friction constant are small. Nevertheless, we have obtained a few results in the actual geometry of Ref. 3 which may be of particular interest. Figure 11 shows the initially straight vortex coming to steady-state motion under the influence of a friction constant similar to that acting in the experiment. One may conclude that a vortex starting from an arbitrary initial configuration should reach its steady-state behavior in a few precession cycles. An incompletely converged calculation of $\langle\Omega\rangle$ and $\langle\dot{Z}\rangle/\alpha$ has been carried out with a friction constant of 0.10, yielding values of 0.0242 s^{-1} and 0.001 44 cm s^{-1}, respectively. When corrections for convergence and friction are applied, the average precession rate becomes (0.0248 ± 0.0002), where the error estimate derives from uncertainties in making the corrections. This corresponds to a calculated precession period of (253 ± 2) s, compared to a theoretical value from Eq. (18) of 252 s. As mentioned at the end of Sec. III, if the calculations were carried out using the more accurate form of Eq. (2) for the circulating field, one would expect to obtain a precession period of about 263 ± 3. Comparison with the experimental result of (253 ± 1) s is only good to about 3% because of uncertainties in the experimental values of r_1, r_2, and (especially) Δ. The agreement between experiment, theory, and computation for this primary parameter is consistent with the estimated uncertainties.

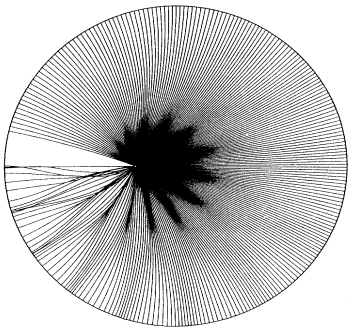

FIG. 11. Transient behavior calculated for the actual geometry of Ref. 3, using $\alpha=0.03$. Steady-state precession is achieved in about one revolution.

A second interesting computational result (Fig. 12) is the oscillation signature that one expects to observe for the geometry of Ref. 3. The calculation was carried out using $\alpha=0.10$, and the unwinding slope was than adjusted to zero. We note that the oscillations are predicted to be noticeably anharmonic, an effect which may be experimentally testable. As discussed in Sec. V, a much more strikingly anharmonic signature could be obtained with a more eccentric placement of the inner wire.

Finally, we have calculated (Figs. 13 and 14) how an individual pinning and release event would appear in the actual experiment. Referring to the discussion of Sec. VI, the effect is somewhat more dramatic for a small-diameter, off-center wire, because the critical depinning angle can be made larger without permanently trapping the vortex. As seen in Fig. 14, the signature of such an event is still not very impressive, but it now looks distinctive enough to be perhaps observable in data of the quality shown in Fig. 1.

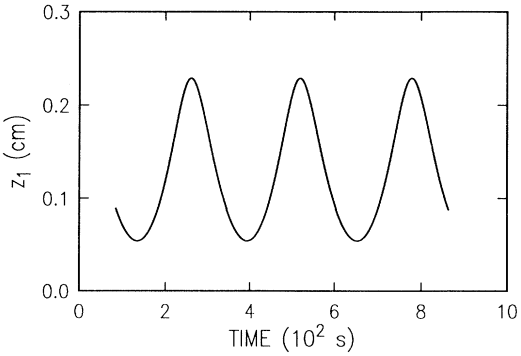

FIG. 12. Oscillation signature expected for the geometry of Ref. 3. The unwinding baseline has been subtracted out.

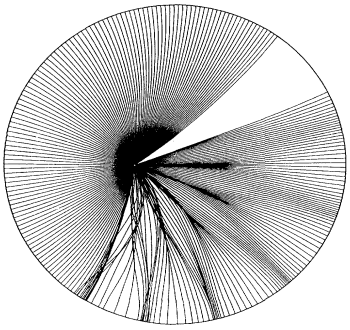

FIG. 13. Vortex motion during a single pinning and depinning event. The critical angle was taken as 40°. The calculation was done with $\alpha=0.03$ and the geometrical parameters of Ref. 3.

VIII. START OF THE UNWINDING PROCESS

An interesting question is how the unwinding process can be initiated. Clearly, a state of uniform circulation along the entire wire is strongly metastable, and it requires a large macroscopic disturbance to go over to the state pictured in Fig. 2. One possible explanation is that the requisite disturbance is provided by a previously extant (remanent) free vortex which encounters the wire while drifting through the fluid, and reconnects as shown in Fig. 15. Both vortices will then unwind, one upward and the other downward. The signature of such an event would consist of some initial period of constant effective circulation, followed by an apparent unwinding rate slowing down from $4\dot{Z}$ to $2\dot{Z}$ as the vortices separate, and then switching to an unwinding rate $\dot{Z}$ when one of the vortices has finished unwinding. It is noteworthy that, with a little good will, Fig. 1 can in fact, be viewed as resembling such a scenario. Other experimental signatures to look for in support of this speculation can be identified. If the two vortices remain exactly 180° out of phase as they precess, there should be little or no oscillatory signal during the fast part of the decay. More generally, a quite complex signal might be observed. Moreover, one might expect the exact location where the remanent vortex reconnects to vary randomly. Thus, the

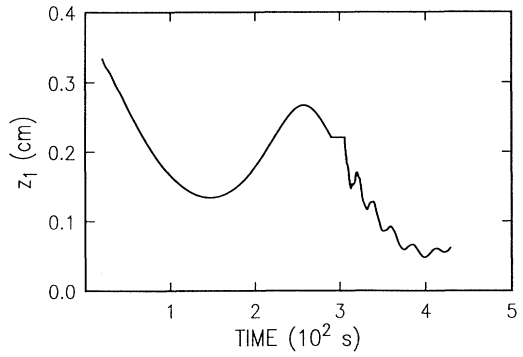

FIG. 14. Experimental signature of the event shown in Fig. 13.

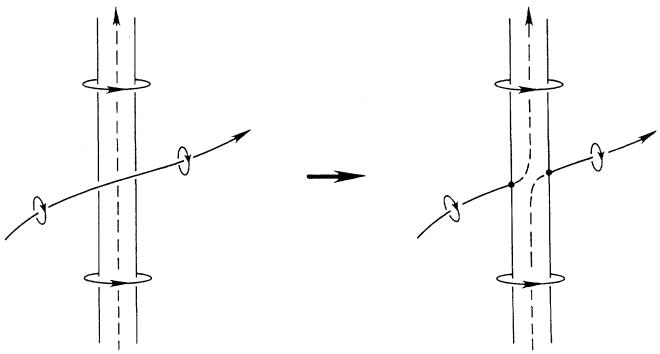

FIG. 15. Schematic view of how the unwinding process could be initiated by a preexisting free vortex.

relative duration of the fast and slow decay intervals may vary randomly over a wide range. Finally, more complex sequences of unwinding could arise if other remanent vortices became involved in the unwinding process, impacting either the wire or the precessing vortex. Observations of such features would put the speculation schematized in Fig. 15 on firmer ground, and could provide an important tool for investigating the existence and the behavior of remanent vorticity.

IX. CONCLUSIONS

The basic picture proffered by Zieve *et al.*[3] of a vortex unwinding from a wire by precessing under the influence of the trapped circulation remaining on the wire is validated by direct calculation of the vortex motion. Their force-balance argument is found to give a good approximation to the rate of precession and rate of unwinding in the limit of small friction constant. Following Misirpashaev and Volovik,[13] this argument can be generalized to the case of an off-center wire. A linearized analysis of the equations of motion permits one to calculate the effect on the precession and unwinding rate of having a nonzero friction constant. It is found that this correction is small in the experimental situation of Ref. 3.

As the inner wire is moved away from the center, the precession becomes increasingly anharmonic and a large oscillating component appears in the vertical unwinding velocity of the vortex. Both the average precession rate and the average unwinding rate are increasingly affected. Good agreement between computations in the limit $\alpha\rightarrow 0$ and the force-balance argument is obtained, provided that image effects are taken into account. These become increasingly important as the eccentricity becomes large, and combine with the friction to produce more complicated kinds of behavior. Very striking experimental effects are predicted to occur when the wire is placed near the outer wall.

The effect of vortex pinning has been investigated using a critical-angle model of the depinning process. Above a maximum depinning angle, the vortex will stop its motion and settle into a permanent pinned state. Since the depinning angle is much smaller on the outer surface than on the wire, roughness of the containing bucket is more effective in immobilizing the vortex than roughness

of the wire. If conditions are set such that pinning and release can occur, the experimental signal will exhibit steplike glitches followed by damped oscillations, which may be observable. However, the most obvious effect of pinning is likely to be a complete disappearance of the oscillating signal as the vortex is immobilized.

For the specific geometry quoted by Zieve *et al.*,[3] the computations using Eq. (6) give a precession period of (253 ± 2) s, compared with the analytical value of 252 s. Computations using the more accurate circulating field of Eq. (2) are projected to give 263 ± 3 s. The experimentally observed value is 253 ± 7 s. This agreement provides the best evidence to date for the applicability of classical vortex-filament dynamics to quantized vortex lines.

ACKNOWLEDGMENTS

The author wishes to thank R. E. Packard for sharing his experimental results with him prior to publication, and for several informative discussions. He also wishes to thank G. E. Volovik and E. Sonin for a series of stimulating and illuminating exchanges.

[1]H. E. Hall and W. F. Vinen, Proc. R. Soc. London, Ser. A **238**, 204 (1956); **238**, 215 (1956).

[2]G. W. Rayfield and F. Reif, Phys. Rev. **136A**, 1194 (1964).

[3]R. J. Zieve, Yu. Mukharsky, J. D. Close, J. C. Davis, and R. E. Packard, Phys. Rev. Lett. **68**, 1327 (1992).

[4]W. F. Vinen, Proc. R. Soc. London, Ser. A **260**, 218 (1961).

[5]P. W. Karn, D. R. Starks, and W. Zimmermann, Jr., Phys. Rev. B **21**, 1797 (1980).

[6]J. C. Davis, J. D. Close, R. Zieve, and R. E. Packard, Phys. Rev. Lett. **66**, 329 (1991).

[7]K. W. Schwarz, Phys. Rev. B **31**, 5782 (1985).

[8]If the wire is placed off center, an important boundary correction *does* arise. This is discussed in Sec. IV.

[9]All of the calculations except those discussed in Sec. VII were done using a standard geometry of $r_1=0.005$ cm and $r_2=0.100$ cm. The use of a relatively large inner radius greatly reduces the amount of computation necessary to simulate the vortex motion.

[10]See, for example, Figs. 14, 18, and 31 in Ref. 7.

[11]K. W. Schwarz, Phys. Rev. B **38**, 2398 (1988).

[12]Note that $f(t)$ has no significance, since a uniform pressure field does not affect the dynamics.

[13]T. Sh. Misirpashaev and G. E. Volovik, Pis'ma Zh. Eksp. Teor. Fiz. **56**, 40 (1992) [JETP Lett. **56**, 41 (1992)]. These authors derive Eq. (18) within the more general context of the ac Josephson equation.